Applied Physics Letters

Ultrafast optical-field-induced photoelectron emission in a vacuum nanoscale gap: An exact analytical formulation

Cite as: Appl. Phys. Lett. **119**, 194101 (2021); https://doi.org/10.1063/5.0061914
Submitted: 30 June 2021 • Accepted: 21 October 2021 • Published Online: 08 November 2021

Yi Luo and Peng Zhang

AIP Publishing

Applied Physics Letters ARTICLE scitation.org/journal/apl

Ultrafast optical-field-induced photoelectron emission in a vacuum nanoscale gap: An exact analytical formulation

Cite as: Appl. Phys. Lett. **119**, 194101 (2021); doi: 10.1063/5.0061914
Submitted: 30 June 2021 · Accepted: 21 October 2021 ·
Published Online: 8 November 2021

View Online Export Citation CrossMark

Yi Luo[a] and Peng Zhang[b]

AFFILIATIONS

Department of Electrical and Computer Engineering, Michigan State University, East Lansing, Michigan 48824-1226, USA

[a]**Present address:** Department of Electrical Engineering, University of Notre Dame, Notre Dame, IN 46656, USA.
[b]**Author to whom correspondence should be addressed:** pz@egr.msu.edu

ABSTRACT

By exactly solving the one-dimensional time-dependent Schrödinger equation, we construct an analytical solution for nonlinear photoelectron emission in a nanoscale metal–vacuum–metal junction driven by a single-frequency laser field, where the impact of image and space charges is neglected. Based on the analytical formulation, we examine the photoelectron energy spectra and emission current under various laser fields and vacuum gap distances. Our calculation shows the transition from direct tunneling to multiphoton induced electron emission as gap distance increases. In the multiphoton regime, the photoemission current density oscillatorily varies with the gap distance, due to the interference of electron waves inside the gap. Our model reveals the energy redistribution of photoelectrons across the two interfaces between the gap and the metals. Additionally, we find that decreasing the gap distance (before entering the direct tunneling regime) tends to extend the multiphoton regime to higher laser intensity. This work provides clear insights into the underlying photoemission mechanisms and spatiotemporal electron dynamics of ultrafast electron transport in nanogaps and may guide the future design of advanced ultrafast nanodevices, such as photoelectron emitters, photodetectors, and quantum plasmonic nanoantennas.

Photoelectron emission from nanostructures triggered by ultrafast optical fields provides access to the direct manipulation of electrons on ultrashort spatiotemporal scales,[1–8] making it attractive to ultrafast microscopy,[9] diffraction,[10] free-electron lasers,[11] hot-electron emitters,[12] and nanovacuum electronic devices.[13–16] Due to the promise for potential applications to ultrafast and highly sensitive photodetection in the room temperature, laser-driven electron emission in the nanometer-scale two-tip junctions has drawn strong recent interest.[17–25] Photoelectron emission and tunneling in nanogaps are also critical to quantum plasmonic dimers,[26,27] molecular nanojunctions,[27] and charge transfer bowtie nanoantennas,[28] as surveyed in a recent review article.[8] Typically, numerical solutions of the time-dependent density function theory[17,23,24,26,27] and Schrödinger equation[25,28] are implemented to study the photoemission in nanogaps, but the underlying emission physics and their nonlinear parametric dependence are not always transparent, especially when transitioning among different emission regimes.

In this work, by exactly solving the time-dependent Schrödinger equation, we present an analytical model for nonlinear ultrafast electron emission and dynamics in a nanoscale metal–vacuum–metal junction driven by a single-frequency laser field. Using the analytical formulation, we investigate the photoelectron transport with various gap distances, laser intensities, wavelengths, and metal materials. Our results provide clear insights into the energy distribution of emitted photoelectron and spatiotemporal emission dynamics inside the metal–vacuum–metal junction.

Our one-dimensional (1D) model (see Fig. 1) considers electrons with initial energy ε emitted from the surface at $x = 0$, under the action of laser field $F_1\cos(\omega t)$, where F_1 is the amplitude of the laser field and ω is the angular frequency. The laser field is assumed to be perpendicular to the flat emitter surface and cuts off abruptly at the surface.[4,25] Note that, by symmetry, electron emission from the surface at $x = d$ can be modeled in the same way (but with an opposite sign of instantaneous laser field). This indicates no net time-averaged photoemission current, but only net instantaneous current is generated in a symmetric nanogap.[26–28] Note further that generating nonzero net time-averaged photocurrent requires some sort of symmetry breaking of the nanogap, e.g., by using dissimilar materials on the two sides of

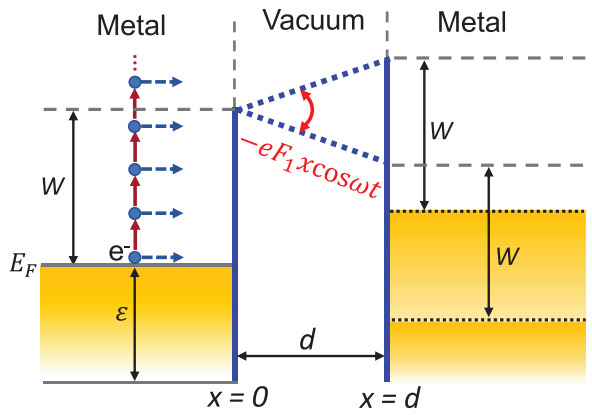

FIG. 1. Energy diagram for photoelectron emission in a nanoscale metal–vacuum–metal junction under a single-frequency laser field. Electrons with the initial energy ε are emitted from the surface at $x=0$, with an energy of $\varepsilon+n\hbar\omega$, due to n-photon contribution.

the gap,[29] dc bias,[17,18,21,25] or spatially or temporally inhomogeneous optical fields.[19,23,24,30] Here, we focus only on a symmetric nanogap, which is applicable to a broad range of plasmonic and ultrafast optoelectronic devices, where direct measurement of the gap current is typically infeasible.[8,26–28] The time-dependent potential energy in Fig. 1 reads[4,5,31–33]

$$\Phi(x,\,t)=\begin{cases}0 & x<0,\\ E_F+W-eF_1x\cos(\omega t) & 0\le x<d,\\ -eF_1d\cos(\omega t) & x\ge d,\end{cases}\tag{1}$$

where E_F and W are the Fermi energy and work function of the left metal, respectively, and e is the elementary charge. Here, the impact of image and space charges is neglected for simplicity.

To obtain the electron emission probability, we solve the time-dependent Schrödinger equation:

$$i\hbar\frac{\partial\psi(x,\,t)}{\partial t}=-\frac{\hbar^2}{2m_e}\frac{\partial^2\psi(x,\,t)}{\partial x^2}+\Phi(x,\,t)\psi(x,\,t),\tag{2}$$

where $\hbar$ is the reduced Plank constant, $\psi(x,\,t)$ is the electron wave function, m_e is the electron mass, and $\Phi(x,\,t)$ is the potential energy given in Eq. (1). For $x<0$, the electron wave function is

$$\psi(x,\,t)=\exp\left(-\frac{i\varepsilon t}{\hbar}+ik_0x\right)+\sum_{n=-\infty}^{\infty}R_n\exp\left(-i\frac{\varepsilon+n\hbar\omega}{\hbar}t-ik_nx\right),\quad x<0,\tag{3}$$

which denotes the superposition of an incident plane wave with initial energy ε and a set of reflected plane waves with reflection coefficient R_n and energies $\varepsilon+n\hbar\omega$, where the wavenumber $k_0=\sqrt{2m_e\varepsilon/\hbar^2}$ and $k_n=\sqrt{2m_e(\varepsilon+n\hbar\omega)/\hbar^2}$.

For $0\le x<d$ (in the gap), the exact solution to Eq. (2) is found to be (see the supplementary material 1 for the method)

$$\psi(x,\,t)=\sum_{n=-\infty}^{\infty}\exp\left[-i\frac{\varepsilon+n\hbar\omega}{\hbar}t\right]\times\exp\left[\frac{ixeF_1\sin(\omega t)}{\hbar\omega}+\frac{ie^2F_1^2\sin(2\omega t)}{8m_e\hbar\omega^3}\right]\times\left\{T_{1n}\exp\left[i\sqrt{\frac{2m_eE_n}{\hbar^2}}\left(x+\frac{eF_1\cos(\omega t)}{m_e\omega^2}\right)\right]+T_{2n}\exp\left[-i\sqrt{\frac{2m_eE_n}{\hbar^2}}\left(x+\frac{eF_1\cos(\omega t)}{m_e\omega^2}\right)\right]\right\},\quad 0\le x<d,\tag{4}$$

which shows the superposition of a set of electron waves traveling toward the $+x$ direction with coefficient T_{1n} and toward the $-x$ direction with coefficient T_{2n} inside the gap, where the drift kinetic energy $E_n=\varepsilon+n\hbar\omega-E_F-W-U_p$ and the ponderomotive energy $U_p=e^2F_1^2/4m_e\omega^2$.

For $x\ge d$, an exact solution of the electron wave function is easily obtained,

$$\psi(x,\,t)=\sum_{n=-\infty}^{\infty}T_{3n}\exp\left(-i\frac{\varepsilon+n\hbar\omega}{\hbar}t\right)\times\exp\left[ik_nx+i\frac{eF_1d\sin(\omega t)}{\hbar\omega}\right],\quad x\ge d,\tag{5}$$

which represents the superposition of transmitted electron plane waves with energies $\varepsilon+n\hbar\omega$, due to multiphoton absorption ($n>0$), direct tunneling ($n=0$), and multiphoton emission ($n<0$),[4,34] where the wavenumber $k_n=\sqrt{2m_e(\varepsilon+n\hbar\omega)/\hbar^2}$, and T_{3n} is the transmission coefficient.

The coefficients T_{1n}, T_{2n}, and T_{3n} (and therefore reflection coefficient R_n) can be calculated from boundary conditions that both the electron wave function $\psi(x,\,t)$ and its derivative $\partial\psi(x,\,t)/\partial x$ are continuous at $x=0$ and $x=d$ (see the supplementary material 2 for details). The normalized transmitted current density is defined as the ratio of the transmitted probability current density over the incident probability current density, $w(\varepsilon,\,x,\,t)=J_t(\varepsilon,\,x,\,t)/J_i(\varepsilon,\,x,\,t)$, where the probability current density is $J(x,\,t)=(i\hbar/2m_e)(\psi\nabla\psi^*-\psi^*\nabla\psi)=(i\hbar/2m_e)\sum_{n=-\infty}^{\infty}\sum_{l=-\infty}^{\infty}(\psi_n\nabla\psi_l^*-\psi_n^*\nabla\psi_l)$. Thus, the normalized instantaneous current density inside the gap ($0<x<d$), in nondimensional quantities,[4,5,31] $\overline{\varepsilon}=\varepsilon/W$, $\overline{\omega}=\omega\hbar/W$, $\overline{t}=tW/\hbar$, $\overline{E}_F=E_F/W$, $\overline{x}=x/\lambda_0$, $\overline{d}=d/\lambda_0$, $\lambda_0=\sqrt{\hbar^2/2m_eW}$, $\overline{F}_1=F_1e\lambda_0/W$, $\overline{U}_p=U_p/W$, and $\overline{E}_n=\overline{\varepsilon}+n\overline{\omega}-\overline{E}_F-\overline{U}_p-1$, is

$$w(\overline{\varepsilon},\,\overline{x},\,\overline{t})=\frac{1}{\sqrt{\overline{\varepsilon}}}\sum_{n=-\infty}^{\infty}\sum_{l=-\infty}^{\infty}Re\left\{e^{i(l-n)\overline{\omega}\overline{t}}\times\left\{T_{1n}T_{1l}^*D_1+T_{1n}T_{2l}^*D_2+T_{2n}T_{1l}^*D_3+T_{2n}T_{2l}^*D_4\right\}\right\},\tag{6}$$

where

$$D_1=\exp\left[i\left(\sqrt{\overline{E}_n}-\left(\sqrt{\overline{E}_l}\right)^*\right)\left(\overline{x}+\frac{2\overline{F}_1\cos(\overline{\omega}\overline{t})}{\overline{\omega}^2}\right)\right]\times\left[\left(\sqrt{\overline{E}_l}\right)^*+\frac{\overline{F}_1\sin(\overline{\omega}\overline{t})}{\overline{\omega}}\right],$$

$$D_2 = -\exp\left[i\left(\sqrt{\bar{E}_n} + \left(\sqrt{\bar{E}_l}\right)^*\right)\left(\bar{x} + \frac{2\bar{F}_1\cos(\bar{\omega}\bar{t})}{\bar{\omega}^2}\right)\right] \times \left[\left(\sqrt{\bar{E}_l}\right)^* - \frac{\bar{F}_1\sin(\bar{\omega}\bar{t})}{\bar{\omega}}\right],$$

$$D_3 = \exp\left[-i\left(\sqrt{\bar{E}_n} + \left(\sqrt{\bar{E}_l}\right)^*\right)\left(\bar{x} + \frac{2\bar{F}_1\cos(\bar{\omega}\bar{t})}{\bar{\omega}^2}\right)\right] \times \left[\left(\sqrt{\bar{E}_l}\right)^* + \frac{\bar{F}_1\sin(\bar{\omega}\bar{t})}{\bar{\omega}}\right],$$

and

$$D_4 = -\exp\left[i\left(\left(\sqrt{\bar{E}_l}\right)^* - \sqrt{\bar{E}_n}\right)\left(\bar{x} + \frac{2\bar{F}_1\cos(\bar{\omega}\bar{t})}{\bar{\omega}^2}\right)\right] \times \left[\left(\sqrt{\bar{E}_l}\right)^* - \frac{\bar{F}_1\sin(\bar{\omega}\bar{t})}{\bar{\omega}}\right].$$

The corresponding time-averaged emission current density is obtained from the numerical integration of Eq. (6) over time,

$$\langle w(\bar{\varepsilon})\rangle = \frac{1}{2\pi}\int_0^{2\pi} w(\bar{\varepsilon}, \bar{x}, \bar{t})d(\bar{\omega}\bar{t}). \quad (7)$$

In the metal on the right-hand side ($x > d$), the normalized instantaneous transmitted current density is found as

$$w(\bar{\varepsilon}, \bar{x}, \bar{t}) = \frac{1}{\sqrt{\bar{\varepsilon}}}\sum_{n=-\infty}^{\infty}\sum_{l=-\infty}^{\infty} Re\left\{e^{i(l-n)\bar{\omega}\bar{t}}T_{3n}T_{3l}^* D\right\}, \quad (8)$$

where $D = e^{i[\sqrt{\bar{\varepsilon}+n\bar{\omega}}-(\sqrt{\bar{\varepsilon}+l\bar{\omega}})^*]\bar{x}}(\sqrt{\bar{\varepsilon}+l\bar{\omega}})^*$. The time-averaged transmitted current density is

$$\langle w(\bar{\varepsilon})\rangle = \sum_{n=-\infty}^{\infty}\langle w_n(\bar{\varepsilon})\rangle, \quad \langle w_n(\bar{\varepsilon})\rangle = \mathrm{Re}\left(|T_{3n}|^2\sqrt{1+n\bar{\omega}/\bar{\varepsilon}}\right), \quad (9)$$

where $\langle w_n\rangle$ represents the time-averaged transmitted current density through the n-photon process, with transmitted electrons of energy $\varepsilon + n\hbar\omega$.[4] Due to current continuity, the time-averaged current density obtained from Eqs. (7) and (9) is equal, which has been verified in our calculations.

Using the analytical solution presented above, we analyze the photoelectron emission properties under different combinations of gap distances and laser fields. Unless mentioned otherwise, the default value of the laser wavelength is 800 nm ($\hbar\omega = 1.55$ eV), the metals on both sides of the gap are assumed to be gold,[17,19–22] with Fermi energy $E_F = 5.53$ eV and work function $W = 5.1$ eV, and the photoemission current is calculated from Eq. (9). Since most of the electrons are emitted with initial energies near the Fermi level,[4,34–36] we choose the electron initial energy $\varepsilon = E_F$ for simplicity.

Figure 2(a) shows the dependence of total time-averaged transmitted current density $\langle w\rangle$ on the gap distance d under different laser fields F_1. When the laser field is off (i.e., $F_1 = 0$), the current $\langle w\rangle$ is contributed only by direct tunneling, which rapidly decreases as gap distance increases. After applying a laser field, the current $\langle w\rangle$ decreases initially as d increases, closely following the scaling for the case of $F_1 = 0$, where direct tunneling dominates. As d increases further, for a given laser field, the current $\langle w\rangle$ oscillates around a constant value (cf. the dashed lines), which is found to be the photoemission current from a single metal surface (i.e., when the metal on the right-hand side in Fig. 1 is removed). The oscillation behavior is attributed to the interference of electron waves inside the gap due to reflections from the metal–vacuum interfaces, for various gap distances d. Here, we ignore the effects of image charge and space charge, thus the oscillation amplitude of $\langle w\rangle$ remains almost unchanged with increasing d. This oscillation behavior is similar to that found in field emission from dielectric coated surfaces.[37] The interference of electron waves is also demonstrated experimentally in Ref. 3, where the distinct peaks in energy spectra arise from electron waves re-scattering at the emitter tip. Notably, using free-electron theory[33] to account for the distribution of electron energy states in the metal, we find the oscillation in emission current density with d is significantly weakened, which indicates that the oscillatory behavior strongly depends on electron ground-state emission channels.[34] Figure 2(b) displays the direct tunneling background current $\langle w\rangle_{DT}$ (i.e., $F_1 = 0$) and current driven by optical field only, which is obtained by subtracting $\langle w\rangle_{DT}$ from the total emission current $\langle w\rangle$ in Fig. 2(a), $\langle w\rangle - \langle w\rangle_{DT}$. It can be seen that after a certain value of d, optically driven current becomes much larger than the tunneling background current, indicating the current is mainly driven by the incident laser field. For instance, for $F_1 = 1$ V/nm (the blue curve), as $d > 1$ nm, the laser-driven electron emission dominates the current in the nanovacuum junction, where the electron direct tunneling is negligible.

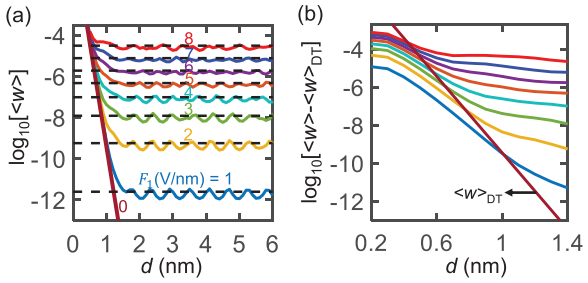

FIG. 2. Normalized time-averaged photoemission current density under various gap sizes and laser fields. (a) Total emission current density $\langle w\rangle$ as a function of gap distance d for different laser fields F_1. Dashed lines denote the emission current density from a single surface when the metal on the right-hand side in Fig. 1 is removed, which is obtained from Ref. 4. (b) Laser field driven emission current $\langle w\rangle - \langle w\rangle_{DT}$ as a function of gap distance d for different laser fields F_1. Here, $\langle w\rangle$ is the emission current in (a). $\langle w\rangle_{DT}$ denotes the direct tunneling background current for $F_1 = 0$ in (a).

Figure 3(a) shows the energy spectra for photoelectrons transmitted into the right-side metal for different gap distances d and laser fields F_1. For a smaller laser field ($F_1 = 1$ V/nm), as d decreases, the dominant emission shifts from four-photon over-barrier emission ($n = 4$, cf. the ratio of the metal work function over single photon energy $W/\hbar\omega \approx 3.29$) to tunneling emission ($n < 4$). As laser field increases ($F_1 = 4$ and 8 V/nm), this shift of the dominant emission process becomes less prominent because the potential barrier inside the gap becomes less sensitive to the gap distance d under strong laser fields. Since the direct tunneling background emission only occurs at $n = 0$ (cf. the vertical solid lines), this observed shift is driven by the incident laser field.

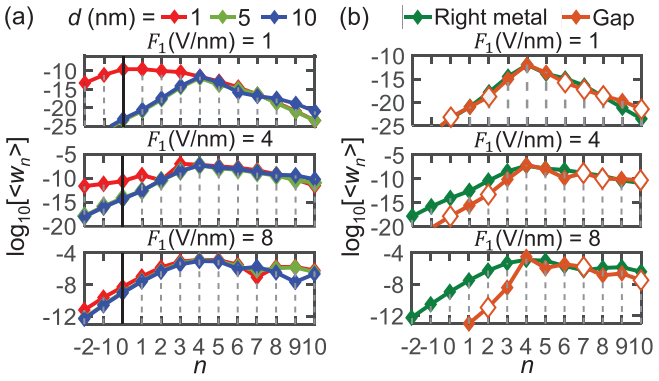

FIG. 3. (a) Energy spectra for photoelectrons transmitted into the metal on the right-hand side for different d and F_1. (b) Photoelectron energy spectra for electrons inside the vacuum gap and in the metal on the right-hand side under different F_1 for $d = 2$ nm. For the curves for photoelectrons inside the gap, white-filled diamond markers denote the absolute value of negative emission current density $\langle w_n \rangle$ through the nth channel.

Figure 3(b) compares the energy spectra for photoelectrons inside the gap and in the right-side metal for $d = 2$ nm. It is found that although the total emission current $\langle w \rangle$ is equal in these two regions, the energy distribution of photoelectrons is quite different. In particular, the time-averaged current densities for all n-photon channels are positive in the right-side metal, while some of them are negative inside the gap [see the open diamond markers in Fig. 3(b)]. Negative value of $\langle w_n \rangle$ means that electrons excited through those n-photon processes are reflected backward inside the gap. Additionally, n-photon processes with $n < 4$ contribute more significantly for transmitted electrons in the right-side metal than those inside the gap, which becomes more pronounced for larger laser intensity.

In Fig. 4(a), we plot the total time-averaged emission current density $\langle w \rangle$ as a function of laser field F_1 with various gap distances d. For the vacuum gap with $d \leq 1$ nm, the slope of $\langle w \rangle$ increases with F_1, indicating that the dominant emission process shifts to higher order n-photon absorption. This is consistent with the results shown in Fig. 3(a). For the cases with larger gap distances, the slope of $\langle w \rangle$ becomes insensitive to the gap distance d and follows that of photoemission current from a single metal surface. The scale approaches $\langle w \rangle \propto F_1^{2n}$ with $n = 4$, indicating that four-photon absorption dominates the emission process. Figure 4(b) displays the difference between the total emission current in a nanogap and emission current from a single surface $\langle w \rangle - \langle w \rangle_{SS}$, where the difference becomes more pronounced in the larger laser intensity regime. Moreover, it is interesting to find that the location of channel closing [i.e., the location of transition between the dominant four- and five-photon absorption in Fig. 4(c), see the supplementary material 3] shifts to larger laser field F_1 for smaller gap distance d. This indicates that decreasing the gap distance (before entering the direct tunneling regime) can extend the multiphoton regime to higher laser intensity. This may be explained by the fact that the shape of the potential barrier becomes less sensitive to the laser field strength for a smaller gap distance, thus allowing the dominant n-photon process to remain over a larger range of laser fields (or laser intensities).

Figure 5 shows the time-dependent current density $w(x, t)$ as a function of space x and time t for different combinations of laser field F_1 and gap distance d. It is seen that, in addition to the surface oscillation current near the metal–vacuum interface at $x = 0$, some electrons are back reflected from the vacuum–metal interface at $x = d$ into the vacuum gap approximately at the beginning of second half cycle of the laser fields (i.e., $\omega t = \pi$). This is shown by the change of $w(x, t)$ from red to dark blue around $\omega t = \pi$ in Figs. 5(e), 5(f), 5(h), and 5(i), where the red region denotes positive current density propagates in the $+x$ direction and the dark blue region in the $-x$ direction. As d increases, more interference patterns of $w(x, t)$ inside the gap are formed. The full width at half maximum (FWHM) of the emission current pulse is about 0.63 fs, which is greatly shorter than laser period of 2.67 fs. Additionally, the nonlinear effects of laser wavelength and materials

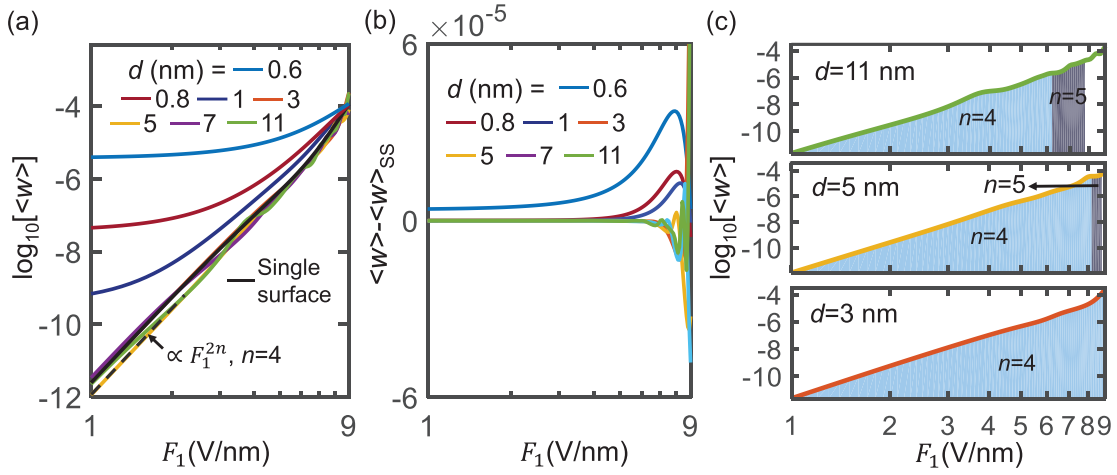

FIG. 4. (a) Normalized total time-averaged emission current density $\langle w \rangle$ and (b) difference between total emission current $\langle w \rangle$ and emission current from a single surface $\langle w \rangle_{SS}$ as a function of laser field F_1 for different gap distances d. The single surface case $\langle w \rangle_{SS}$ is obtained from Ref. 4. The dashed line in (a) denotes the scale of $\langle w \rangle \propto F_1^{2n}$ with $n = 4$. (c) $\langle w \rangle$ as a function of F_1 for $d = 3$, 5, and 11 nm. Here, laser field regimes are labeled with $n = 4$ and $n = 5$ (cf. the areas filled with different colors), which means the dominant emission process in this field regime is four- or five- photon absorption, respectively.

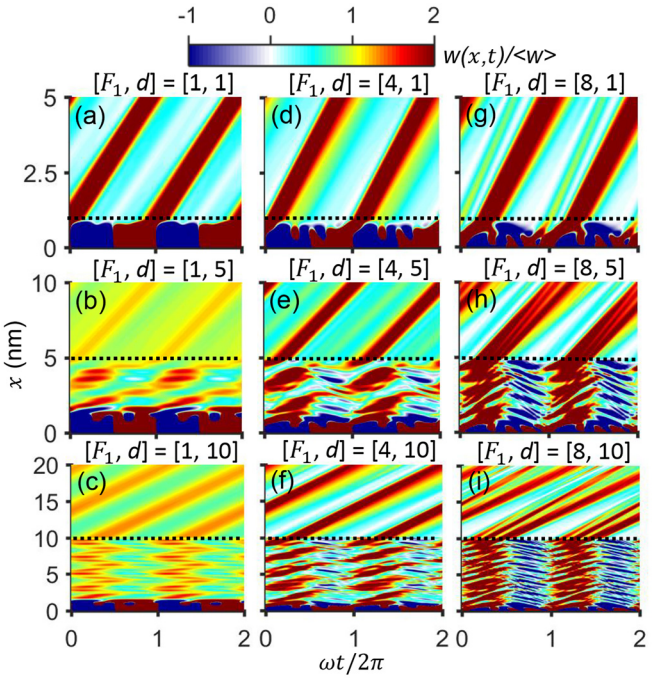

FIG. 5. Total time-dependent current density $w(x,t)$ as a function of time t and space x, under various laser fields F_1 and gap distances d. Here, the time-dependent current density $w(x,t)$ is normalized in terms of the time-averaged current density $\langle w \rangle$. In all figures, the units of F_1 and d are V/nm and nm, respectively. The dotted lines show the position of $x = d$.

on the gap-size dependence of total time-averaged emission current are discussed in the supplementary material 4. The results indicate that for a given laser wavelength and intensity, the transition from direct tunneling to multiphoton emission occurs at a smaller gap spacing for nanogaps formed with smaller work functions.

In summary, we present an analytical solution for photoelectron emission and transport in a nanoscale metal–vacuum–metal junction driven by a single-frequency laser field, by exactly solving the time-dependent Schrödinger equation. The analytical model is valid for arbitrary gap distance, laser intensity (below the material damage threshold), wavelength (of photon energy below the ionization threshold of the metal atom), and the metal work function and Fermi level. Our calculation exhibits the transition from direct tunneling to multiphoton induced electron emission and the oscillatory dependence of photoemission current on the gap distance in the multiphoton regime. Our results demonstrate the energy redistribution of emitted photoelectrons across the two interfaces of the nanogap. We also find that decreasing the gap distance (but before transiting into the direct tunneling regime) can extend the multiphoton regime to higher laser intensity. Our work would be useful for understanding underlying photoemission mechanisms and spatiotemporal electron dynamics of ultrafast electron transport in nanogaps, which have applications in quantum plasmonics, quantum nano-optics, nanoantennas, ultrafast optoelectronics, and ultrafast photodetectors such as hot carrier photodetection using metal nanoparticles.[38,39]

Future work will consider the impact of dc bias,[4,5,25] nonlinear field enhancement near higher dimensional emitter tips,[14] surface structures, roughness, and defects, pulsed laser excitation,[7] and laser heating effects. The effects of plasmonic resonance[6,20,26–28,30] as well as surface coating[6,37] may also be considered. It would be interesting to examine nanogaps formed with semiconductors[38,39] or low-dimensional materials. The effects of rectification in nanogaps formed with dissimilar materials[29] require further investigation. Our current model ignores image charge, exchange–correlation, space charge effects,[16,29,36] laser field penetration inside the metal electrodes, and laser heating (Ref. 40) which are expected to change the characteristics of current transport and need to be studied in the future.

See the supplementary material for the derivation of the exact solution of the electron wave function, the calculation of transmission and reflection coefficients, photoelectron energy spectra for different gap distances, and effects of laser wavelength and materials on photoemission.

This work was supported by Air Force Office of Scientific Research (AFOSR) YIP Grant (No. FA9550-18-1-0061) and Office of Naval Research (ONR) YIP Grant (No. N00014-20-1-2681).

AUTHOR DECLARATIONS

Conflict of Interest

The authors have no conflicts of interest to disclose.

DATA AVAILABILITY

The data that support the findings of this study are available from the corresponding author upon reasonable request.

REFERENCES

[1]P. Hommelhoff, C. Kealhofer, and M. A. Kasevich, "Ultrafast electron pulses from a tungsten tip triggered by low-power femtosecond laser pulses," Phys. Rev. Lett. **97**, 247402 (2006).
[2]R. Bormann, M. Gulde, A. Weismann, S. V. Yalunin, and C. Ropers, "Tip-enhanced strong-field photoemission," Phys. Rev. Lett. **105**, 147601 (2010).
[3]M. Krüger, M. Schenk, and P. Hommelhoff, "Attosecond control of electrons emitted from a nanoscale metal tip," Nature **475**, 78 (2011).
[4]P. Zhang and Y. Y. Lau, "Ultrafast strong-field photoelectron emission from biased metal surfaces: Exact solution to time-dependent Schrödinger equation," Sci. Rep. **6**, 19894 (2016).
[5]Y. Luo and P. Zhang, "Analysis of two-color laser-induced electron emission from a biased metal surface using an exact quantum mechanical solution," Phys. Rev. Appl. **12**, 044056 (2019).
[6]X. Xiong, Y. Zhou, Y. Luo, X. Li, M. Bosman, L. K. Ang, P. Zhang, and L. Wu, "Plasmon-enhanced resonant photoemission using atomically thick dielectric coatings," ACS Nano **14**, 8806 (2020).
[7]Y. Luo, Y. Zhou, and P. Zhang, "Few-cycle optical-field induced photoemission from biased surfaces: An exact quantum theory," Phys. Rev. B **103**, 085410 (2021).
[8]P. Dombi, Z. Pápa, J. Vogelsang, S. V. Yalunin, M. Sivis, G. Herink, S. Schäfer, P. Groß, C. Ropers, and C. Lienau, "Strong-field nano-optics," Rev. Mod. Phys. **92**, 025003 (2020).
[9]S. Sun, X. Sun, D. Bartles, E. Wozniak, J. Williams, P. Zhang, and C.-Y. Ruan, "Direct imaging of plasma waves using ultrafast electron microscopy," Struct. Dyn. **7**, 064301 (2020).
[10]G. Sciaini and R. J. D. Miller, "Femtosecond electron diffraction: Heralding the era of atomically resolved dynamics," Rep. Prog. Phys. **74**, 096101 (2011).
[11]I. Grguraš, A. R. Maier, C. Behrens, T. Mazza, T. J. Kelly, P. Radcliffe, S. Düsterer, A. K. Kazansky, N. M. Kabachnik, T. Tschentscher, J. T. Costello, M. Meyer, M. C. Hoffmann, H. Schlarb, and A. L. Cavalieri, "Ultrafast x-ray pulse characterization at free-electron lasers," Nat. Photonics **6**, 852 (2012).

[12]F. Rezaeifar, R. Ahsan, Q. Lin, H. U. Chae, and R. Kapadia, "Hot-electron emission processes in waveguide-integrated graphene," Nat. Photonics **13**, 843 (2019).
[13]P. Zhang and Y. Y. Lau, "Ultrafast and nanoscale diodes," J. Plasma Phys. **82**, 595820505 (2016).
[14]J. Lin, P. Y. Wong, P. Yang, Y. Y. Lau, W. Tang, and P. Zhang, "Electric field distribution and current emission in a miniaturized geometrical diode," J. Appl. Phys. **121**, 244301 (2017).
[15]P. Zhang, Á. Valfells, L. K. Ang, J. W. Luginsland, and Y. Y. Lau, "100 Years of the physics of diodes," Appl. Phys. Rev. **4**, 011304 (2017).
[16]P. Zhang, Y. S. Ang, A. L. Garner, A. Valfells, J. W. Luginsland, and L. K. Ang, "Space-charge limited current in nanodiodes: Ballistic, collisional and dynamical effects," J. Appl. Phys. **129**, 100902 (2021).
[17]D. R. Ward, F. Hüser, F. Pauly, J. C. Cuevas, and D. Natelson, "Optical rectification and field enhancement in a plasmonic nanogap," Nat. Nanotechnol. **5**, 732 (2010).
[18]T. Higuchi, L. Maisenbacher, A. Liehl, P. Dombi, and P. Hommelhoff, "A nanoscale vacuum-tube diode triggered by few-cycle laser pulses," Appl. Phys. Lett. **106**, 051109 (2015).
[19]T. Rybka, M. Ludwig, M. F. Schmalz, V. Knittel, D. Brida, and A. Leitenstorfer, "Sub-cycle optical phase control of nanotunnelling in the single-electron regime," Nat. Photonics **10**, 667 (2016).
[20]P. Rácz, Z. Pápa, I. Márton, J. Budai, P. Wróbel, T. Stefaniuk, C. Prietl, J. R. Krenn, and P. Dombi, "Measurement of nanoplasmonic field enhancement with ultrafast photoemission," Nano Lett. **17**, 1181 (2017).
[21]S. Piltan and D. Sievenpiper, "Plasmonic nano-arrays for enhanced photoemission and photodetection," J. Opt. Soc. Am. B **35**, 208 (2018).
[22]J. Heimerl, T. Higuchi, M. Ammon, M. A. Schneider, and P. Hommelhoff, "Gap-size dependence of optical near fields in a variable nanoscale two-tip junction," Phys. Rev. B **101**, 125403 (2020).
[23]M. Ludwig, G. Aguirregabiria, F. Ritzkowsky, T. Rybka, D. C. Marinica, J. Aizpurua, A. G. Borisov, A. Leitenstorfer, and D. Brida, "Sub-femtosecond electron transport in a nanoscale gap," Nat. Phys. **16**, 341 (2020).
[24]M. Ludwig, A. K. Kazansky, G. Aguirregabiria, D. C. Marinica, M. Falk, A. Leitenstorfer, D. Brida, J. Aizpurua, and A. G. Borisov, "Active control of ultrafast electron dynamics in plasmonic gaps using an applied bias," Phys. Rev. B **101**, 241412 (2020).
[25]M. Turchetti, M. R. Bionta, Y. Yang, F. Ritzkowsky, D. R. Candido, M. Flatté, K. K. Berggren, and P. D. Keathley, "Impact of DC bias on weak optical-field-driven electron emission in nano-vacuum-gap detectors," J. Opt. Soc. Am. B **38**, 1009 (2021).
[26]D. C. Marinica, A. K. Kazansky, P. Nordlander, J. Aizpurua, and A. G. Borisov, "Quantum plasmonics: Nonlinear effects in the field enhancement of a plasmonic nanoparticle dimer," Nano Lett. **12**, 1333 (2012).
[27]W. Zhu, R. Esteban, A. G. Borisov, J. J. Baumberg, P. Nordlander, H. J. Lezec, J. Aizpurua, and K. B. Crozier, "Quantum mechanical effects in plasmonic structures with subnanometre gaps," Nat. Commun. **7**, 11495 (2016).
[28]L. Wu, H. Duan, P. Bai, M. Bosman, J. K. W. Yang, and E. Li, "Fowler-Nordheim tunneling induced charge transfer plasmons between nearly touching nanoparticles," ACS Nano **7**, 707 (2013).
[29]S. Banerjee and P. Zhang, "A generalized self-consistent model for quantum tunneling current in dissimilar metal-insulator-metal junction," AIP Adv. **9**, 085302 (2019).
[30]P. Zimmermann, A. Hötger, N. Fernandez, A. Nolinder, K. Müller, J. J. Finley, and A. W. Holleitner, "Toward plasmonic tunnel gaps for nanoscale photoemission currents by on-chip laser ablation," Nano Lett. **19**, 1172 (2019).
[31]Y. Luo and P. Zhang, "Ultrafast strong-field photoelectron emission due to two-color laser fields," Phys. Rev. B **98**, 165442 (2018).
[32]Y. Luo, J. Luginsland, and P. Zhang, "Interference modulation of photoemission from biased metal cathodes driven by two lasers of the same frequency," AIP Adv. **10**, 075301 (2020).
[33]Y. Zhou and P. Zhang, "A quantum model for photoemission from metal surfaces and its comparison with the three-step model and Fowler–DuBridge Model," J. Appl. Phys. **127**, 164903 (2020).
[34]S. V. Yalunin, M. Gulde, and C. Ropers, "Strong-field photoemission from surfaces: Theoretical approaches," Phys. Rev. B **84**, 195426 (2011).
[35]J. W. Gadzuk and E. W. Plummer, "Field emission energy distribution (FEED)," Rev. Mod. Phys. **45**, 487 (1973).
[36]P. Zhang, "Scaling for quantum tunneling current in nano- and subnano-scale plasmonic junctions," Sci. Rep. **5**, 9826 (2015).
[37]Y. Zhou and P. Zhang, "Theory of field emission from dielectric coated surfaces," Phys. Rev. Res. **2**, 043439 (2020).
[38]L. Chen, S. Mao, P. Wang, Z. Yao, Z. Du, Z. Zhu, L. A. Belfiore, and J. Tang, "Visible light driven hot-electron injection by Pd nanoparticles: Fast response in metal–semiconductor photodetection," Adv. Opt. Mater. **9**, 2001505 (2021).
[39]Y. Zhu, H. Xu, P. Yu, and Z. Wang, "Engineering plasmonic hot carrier dynamics toward efficient photodetection," Appl. Phys. Rev. **8**, 021305 (2021).
[40]Y. Zhou and P. Zhang, "Quantum efficiency of photoemission from biased metal surfaces with laser wavelengths from UV to NIR," J. Appl. Phys. **130**, 064902 (2021).

Supplemental Materials for

Ultrafast optical-field-induced photoelectron emission in a vacuum nanoscale gap: an exact analytical formulation

Yi Luo[1+], and Peng Zhang[1]*

[1]Department of Electrical and Computer Engineering, Michigan State University, East Lansing, Michigan 48824-1226, USA
[+]Present address: Department of Electrical Engineering, University of Notre Dame, Notre Dame, IN 46656, USA.
*e-mail: pz@egr.msu.edu

Supplement 1: Exact solution of electron wave function

Following Truscott[1,2], the time dependent potential for $0 \le x < d$ could be written as $\Phi(x,t) = V(x,t) - xf(t)$, with $V(x,t) = E_F + W$, and $f(t) = eF_1\cos(\omega t)$. Thus, Eq. (2) in the main text could be transformed to the coordinate system ξ, t, where $\xi = x - q(t)$, the displacement $q(t) = (1/m_e)\int^t p(t')dt'$, and $p(t) = \int^t f(t')dt'$, by assuming that $\psi(x,t) = \phi(\xi,t)\chi(x,t)$, with $\chi(x,t) = \exp[-iEt/\hbar + ixp(t)/\hbar - (i/2\hbar m_e)\int^t p^2(t')dt']$, and E being a constant. We have,

$$i\hbar\frac{\partial\phi(\xi,t)}{\partial t} = \left[-\frac{\hbar^2}{2m_e}\frac{\partial^2}{\partial\xi^2} + U(\xi,t) - E\right]\phi(\xi,t), \tag{S1}$$

with $U(\xi,t) = V(x,t)$. By separation of variables, Eq. (S1) can be easily solved to give

$$\phi(\xi,t) = \phi(\xi) = e^{\pm i\xi\sqrt{2m_e(E-V_0)/\hbar^2}}, \tag{S2}$$

Here, "+" in $\phi(\xi)$ denotes the electron wave travelling towards +x direction; "–" denotes the electron wave travelling towards –x direction. Due to the reflection of electron waves at metal-vacuum surfaces of x=0 and d (see Fig. 1), the electron wave function $\psi(x,t)$ inside the vacuum gap ($0 < x < d$) should be the superposition of wave functions towards +x direction and –x direction. Then, from $\psi(x,t) = \phi(\xi)\chi(x,t)$, we obtain Eq. (4), which is the exact solution to Eq. (2), upon using $E = \varepsilon + n\hbar\omega - e^2F_1^2/4m_e\omega^2$.

Supplement 2: Calculation of transmission and reflection coefficients

By imposing the boundary conditions that both the electron wave function $\psi(x,t)$ and its derivative $\partial\psi(x,t)/\partial x$ are continuous at x = 0 and x = d, and taking Fourier transform, we obtain, in nondimensional quantities defined in the main text above Eq. (6)[2,3,4], the following equations,

$$\sum_{n=-\infty}^{\infty} T_{1n}\left[\sqrt{\bar{\varepsilon}+m\bar{\omega}}P_{1n(n-m)} + Q_{1n(n-m)}\right] + T_{2n}\left[\sqrt{\bar{\varepsilon}+m\bar{\omega}}P_{2n(n-m)} + Q_{2n(n-m)}\right] = 2\sqrt{\bar{\varepsilon}}\delta(m) \tag{S3}$$

$$\sum_{n=-\infty}^{\infty}[\sqrt{\bar{\varepsilon}+m\bar{\omega}}U_{1n(n-m)}-V_{1n(n-m)}]T_{1n}+\left[\sqrt{\bar{\varepsilon}+m\bar{\omega}}U_{2n(n-m)}-V_{2n(n-m)}\right]T_{2n}=0 \tag{S4}$$

$$\sum_{n=-\infty}^{\infty}T_{1n}\,U_{1n(n-m)}+T_{2n}U_{2n(n-m)}=\;T_{3m}\exp\left(i\bar{d}\sqrt{\bar{\varepsilon}+m\bar{\omega}}\right) \tag{S5}$$

where $\delta(m)$, $P_{1n(n-m)}$, $Q_{1n(n-m)}$, $P_{2n(n-m)}$, $Q_{2n(n-m)}$, $U_{1n(n-m)}$, $V_{1n(n-l)}$, $U_{2n(n-m)}$, and $V_{2n(n-l)}$ are given by,

$$\delta(m)=\begin{cases}1, & m=0,\\ 0, & m\neq 0,\end{cases} \tag{S6a}$$

$$P_{1nl}=\frac{1}{2\pi}\int_0^{2\pi}p_{1n}(\bar{\omega}\bar{t})e^{-il\bar{\omega}\bar{t}}d(\bar{\omega}\bar{t}),\;\; Q_{1nl}=\frac{1}{2\pi}\int_0^{2\pi}q_{1n}(\bar{\omega}\bar{t})e^{-il\bar{\omega}\bar{t}}d(\bar{\omega}\bar{t}), \tag{S6b}$$

$$P_{2nl}=\frac{1}{2\pi}\int_0^{2\pi}p_{2n}(\bar{\omega}\bar{t})e^{-il\bar{\omega}\bar{t}}d(\bar{\omega}\bar{t}),\;\; Q_{2nl}=\frac{1}{2\pi}\int_0^{2\pi}q_{2n}(\bar{\omega}\bar{t})e^{-il\bar{\omega}\bar{t}}d(\bar{\omega}\bar{t}), \tag{S6c}$$

$$p_{1n}(\bar{\omega}\bar{t})=\mathrm{e}^{i\frac{2\sqrt{\bar{E}_n}\bar{F}_1}{\bar{\omega}^2}\cos(\bar{\omega}\bar{t})}f(\bar{\omega}\bar{t}), \tag{S6d}$$

$$q_{1n}(\bar{\omega}\bar{t})=\left[\sqrt{\bar{E}_n}+\frac{\bar{F}_1}{\bar{\omega}}\sin(\bar{\omega}\bar{t})\right]p_{1n}(\bar{\omega}\bar{t}), \tag{S6e}$$

$$p_{2n}(\bar{\omega}\bar{t})=\mathrm{e}^{-i\frac{2\sqrt{\bar{E}_n}\bar{F}_1}{\bar{\omega}^2}\cos(\bar{\omega}\bar{t})}f(\bar{\omega}\bar{t}), \tag{S6f}$$

$$q_{2n}(\bar{\omega}\bar{t})=\left[\frac{\bar{F}_1}{\bar{\omega}}\sin(\bar{\omega}\bar{t})-\sqrt{\bar{E}_n}\right]p_{2n}(\bar{\omega}\bar{t}), \tag{S6g}$$

$$f(\bar{\omega}\bar{t})=\mathrm{e}^{i\frac{\bar{F}_1{}^2}{4\bar{\omega}^3}\sin(2\bar{\omega}\bar{t})}, \tag{S6h}$$

$$U_{1nl}=P_{1nl}\mathrm{e}^{i\sqrt{\bar{E}_n}\,\bar{d}},\qquad V_{1nl}=Q_{1nl}\mathrm{e}^{i\sqrt{\bar{E}_n}\,\bar{d}}, \tag{S6i}$$

$$U_{2nl}=P_{2nl}\mathrm{e}^{-i\sqrt{\bar{E}_n}\,\bar{d}},\quad V_{2nl}=Q_{2nl}\mathrm{e}^{-i\sqrt{\bar{E}_n}\,\bar{d}}, \tag{S6j}$$

with $\bar{E}_n=\bar{\varepsilon}+n\bar{\omega}-\bar{E}_F-\bar{U}_p-1$. The coefficients T_{1n}, T_{2n}, and T_{3n} (and therefore R_n) is then calculated from Eqs. (S3), (S4) and (S5).

Supplement 3: Photoelectron energy spectra for the gap distance *d* = 3, 5 and 11 nm

In Fig. S1, we plot the energy spectra near the channel closing regime for the gap distances d = 11, 5 and 3 nm. It is clear that for d = 5 and 11 nm, the channel closing (i.e., the transmission between the dominant four- and five- photon absorption) occurs when the laser field F_1 = 8.2 V/nm and 6.2 V/nm, respectively. For d = 3 nm, the dominant emission process is found to be four-photon absorption when F_1 is between 1 and 9 V/nm.

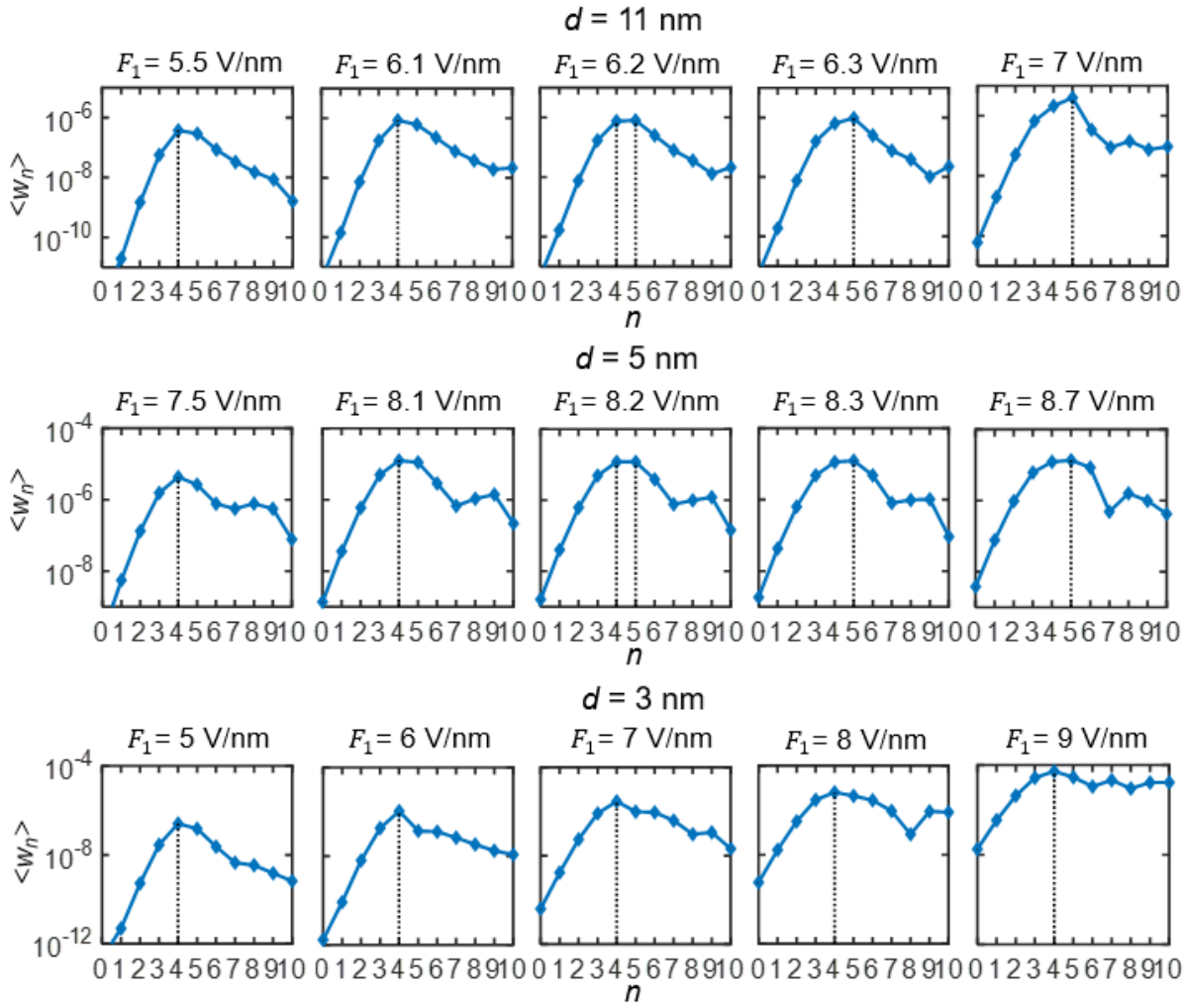

Fig. S1. Photoelectron energy spectra with different laser fields F_1 for the gap distance d = 3, 5 and 11 nm.

Supplement 4: Effects of laser wavelength and materials on the gap-size dependence of total time-averaged emission current

We examine the total time-averaged emission current density $\langle w \rangle$ as a function of gap distance d for different incident wavelengths in Fig. S2(a) and for metals with various work functions in Fig. S2(b). It is found that the oscillation amplitude of $\langle w \rangle$ increases when the laser photon energy $\hbar\omega$ ($\propto 1/\lambda$, with λ being the laser wavelength) becomes closer to the metal work function W, indicating stronger interference of electron waves inside the gap when $W/\hbar\omega \to 1$. Figures S2(c) and S2(d) show the photoelectron energy spectra for different laser wavelengths in Fig. S2(a) and for different metals in Fig. S2(b) with d = 2 nm, respectively. The shift of the dominant emission to larger n-photon process is due to the increasing

ratio of $W/\hbar\omega$. Figure S2(e) displays the energy spectra with different gap distances d for different metals when laser field F_1 = 1 V/nm. Similar to Fig. 3(a), it can be seen that as the gap distance d increases, the general trend is that the main emission process gradually shifts from direct tunneling to multiphoton induced over-barrier emission. It is important to note that, when the gap distance d is small (= 1 nm), the dominant emission for metals with larger work function (i.e., Mo, Cu and Pt) remains as direct tunneling emission (n = 0), whereas the dominant emission process for metals with smaller work function (i.e., Ag and W) becomes multiphoton over-barrier emission (cf. the vertical solid lines). This indicates that, for a given laser wavelength and intensity, the transition from direct tunneling to multiphoton emission occurs at a smaller gap spacing for nanogaps formed with smaller work functions.

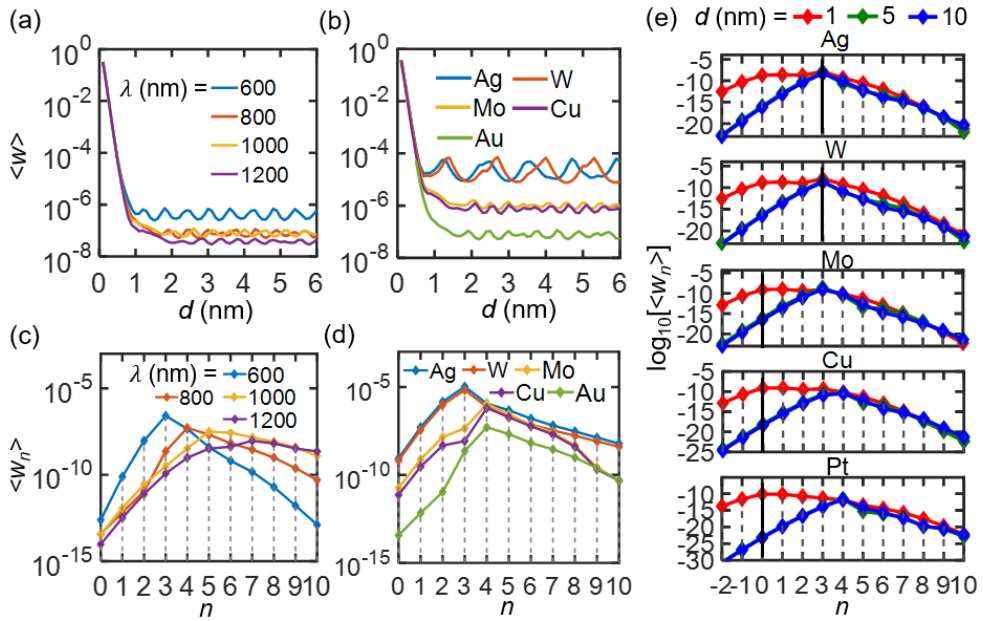

Fig. S2. Normalized total time-averaged emission current density $\langle w \rangle$ as a function of gap distance d for various (a) laser wavelengths and (b) metal materials. Photoelectron energy spectra for different (c) laser wavelengths and (d) metals, for d = 2 nm. (e) Energy spectra for different gap distances d and metals. In (a) and (c), the metal is assumed to be gold. In (b), (d) and (e), the incident wavelength is 800 nm. The work function of different materials is W_{Ag} = 4.26 eV[5], W_W = 4.31 eV[6], W_{Mo} = 4.6 eV[5], W_{Cu} = 4.65 eV[5], W_{Au} = 5.1 eV[2,5], and W_{Pt} = 5.65 eV[5]. The laser field F_1 is fixed as 4 V/nm in (a), (b), (c) and (d) and 1 V/nm in (e), respectively.

References:

[1] W. S. Truscott, Phys. Rev. Lett. **70**, 1900 (1993).

[2] P. Zhang and Y. Y. Lau, Scientific Reports **6**, 19894 (2016).

[3] Y. Luo and P. Zhang, Phys. Rev. Applied **12**, 044056 (2019).

[4] Y. Luo and P. Zhang, Phys. Rev. B **98**, 165442 (2018).

[5] H. B. Michaelson, Journal of Applied Physics **48**, 4729 (1977).

[6] Y. Luo, J. Luginsland, and P. Zhang, AIP Advances **10**, 075301 (2020).